The Effect of Bending on the Critical Current of ReBCO Based Stack Cables

High Magnetic Fields for Muon Collider

UNIVERSITY OF TWENTE.

Author: Nienke Buskens
Date: 2023-06-29
Bachelor Assignment Advanced Technology
Supervisors: Anna Kario & Simon Otten
External Committee Member: Arie van Houselt
University of Twente - Energy Materials & Systems

Abstract

The muon collider is a proposed particle accelerator in which collisions with very high energies can be performed. With these collisions, information can be gathered on the elementary particles. In the muon collider various magnets are needed, of which the target and capture magnet is one of the most complex ones. This magnet requires an operating field of 20 T, a diameter of 1.2 meters and a length of 20 meters. To generate fields of this magnitude superconductors are used. Currently, the ReBCO High-Temperature Superconductor is being researched for its great operating range. Unfortunately, ReBCO is a brittle material so it is important to study the mechanical limits of this material. Especially because these magnets experience high Lorentz forces. ReBCO is made in the form of tapes and these tapes can be stacked to achieve a high current. However, stacking tapes also decreases the flexibility of the cable. In this study, the bending limits of stack cables are studied experimentally while focusing on the dependence of the amount of tapes in the stack on these bending limits. In this work, soldered stack cables of 5 and 10 tapes were chosen according to calculated strain limits. The cables were made using a designed and manufactured soldering tool. In the experiments, these two cables were compared, which showed that the 10-tape stack experienced more critical current degradation than the 5-tape stack for the three different bending radii that were tested. The 5-tape stack showed limited degradation for R=250 mm and R=150 mm, but only 10% critical current remained for R=50 mm. The 10-tape stack showed significant degradation for R=250 mm and R=150 mm, and only 1% critical current remained for R=50 mm. After bending both cables to the radius of 50 mm, visible damage in the form of separation between the tapes was observed in both cables.

List of Abbreviations and Symbols

CERN	European Council for Nuclear Research
ENEA	Italian National Agency for new technologies, energy and sustainable economic development
HTS	High-Temperature Superconductor
LHC	Large Hadron Collider
LN_2	liquid nitrogen
LTS	Low-Temperature Superconductor
ReBCO	rare-earth barium copper oxide
RF	radiofrequency
s.f.	self-field
VI	voltage-current
VIPER	vacuum pressure impregnated, insulated, partially transposed and roll-formed
YBCO	yttrium barium copper oxide

B	magnetic field strength
$\vec{B}$	magnetic field
B_c	critical magnetic field strength
c	lattice constant
d	thickness
E_c	critical electric field
I_c	critical current
J	current density magnitude
J_c	critical current density
$\vec{J}$	current density
F_L	Lorentz force
R	radius
T_c	critical temperature
V_c	critical voltage
y_n	y-coordinate of neutral axis
y_REBCO	y-coordinate of ReBCO tape
σ_θ	hoop stress
θ	angle between magnetic field and tape normal

Contents

1 Introduction

Using superconductors high magnetic fields can be produced. These magnetic fields are useful in several applications, including particle accelerators, nuclear fusion and MRI machines. This study is focused on the application in a muon collider, with which research in fundamental physics can be performed and more information on the elementary particles can be achieved. For a superconductor to be suitable for a magnet, it needs to have good mechanical properties to withstand stress resulting from Lorentz forces. Additionally, it needs to carry a high enough current to establish a high magnetic field. To achieve these high currents, ReBCO is manufactured into stack cables. This report discusses critical current limitation in a ReBCO superconductor as a result of bending a stack cable. These stack cables are made of the ReBCO high-temperature superconductor, a material that is currently being researched for its application in magnets. The stacks are wound into coils, resulting in bending strain. Excessive bending strain can damage the ReBCO tape, resulting in degraded coil performance. Therefore, the bending limits need to be studied experimentally. In this study, such a stack cable is designed and analysed using simulations and experiments. This contains bending the stack cable and studying the effect on the critical current. The study is performed within the Advanced Technology Bachelor assignment framework at the Energy Materials and Systems research group. The research is part of the muon collider european project.

1.1 Standard Model of Particle Physics

Before describing the muon collider, it is important to understand the different particles that are involved. These particles are described in the Standard Model of Particle Physics, which classifies all known elementary particles (Fig. 1.1). The model also describes all the fundamental forces, except for gravity.

One of these elementary particles is the muon. As presented in Fig. 1.1 the muon is a fermion and it carries an electric charge of -1e. The electron falls into this same class, but a muon is 200 times heavier than an electron, which is also given in Fig. 1.1.

Muons can be produced from pions, which consist of a quark and an antiquark. Pions are very unstable and decay after about 26 nanoseconds. A charged pion often decays into muons and muon neutrinos and are thus a suitable source to produce muons.

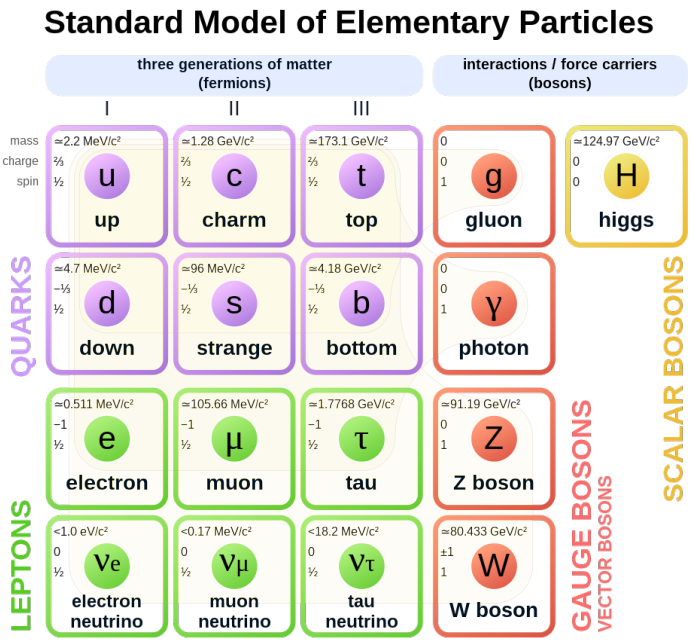

Figure (1.1) *Standard Model of Particle Physics [1].*

.

1.2 Muon collider

The muon collider [2] is a proposed particle accelerator that accelerates muons and makes them collide with each other. During this collison, particles are formed that are analysed using detectors. This way, information on the elementary particles in the Standard Model or beyond can be achieved. The muon collider is different from the Large Hadron Collider (LHC) at CERN, because in the LHC protons are accelerated, which is a composite particle that is very heavy but not very compact. Electrons and muons are elementary particles, so their energy is concentrated in a very small volume [3]. This high energy density together with the fact that muons have a mass that is 200 times larger than that of electrons makes it very suitable for a particle accelerator. Particles with a higher mass generate more collision energy, following Einsteins $E = mc^2$, and therefore a muon collider initiates collisions that generate more energy. The main goal of the muon collider is to get more information on the Higgs boson, one of the elementary particles in Fig. 1.1, and perhaps find undiscovered elementary particles. Apart from the higher collision energy, the proposed muon collider is much smaller than other proposed accelerators using electrons and protons.

Currently, the muon collider is still a proposed machine and it has not been built yet, because it is a large-scale project and not enough research has been done. Therefore, it is in its design phase, and there are many different parts that are being researched. Next, a short description of the design of a muon collider is given.

One specific design [4] for the muon collider is being considered (Fig. 1.2). The generation of a muon beam needs to happen very fast because muons decay after 2.2 micro seconds. Producing muons starts with the production of a proton beam using a proton driver. This beam is compressed into intense and short proton bunches by an accumulator. Using a high-field solenoid, the pions are captured and guided in a decay channel. Next, the beam is cooled to make sure it can be accelerated. Last, the beam is accelerated until it has enough energy to enter the collider ring.

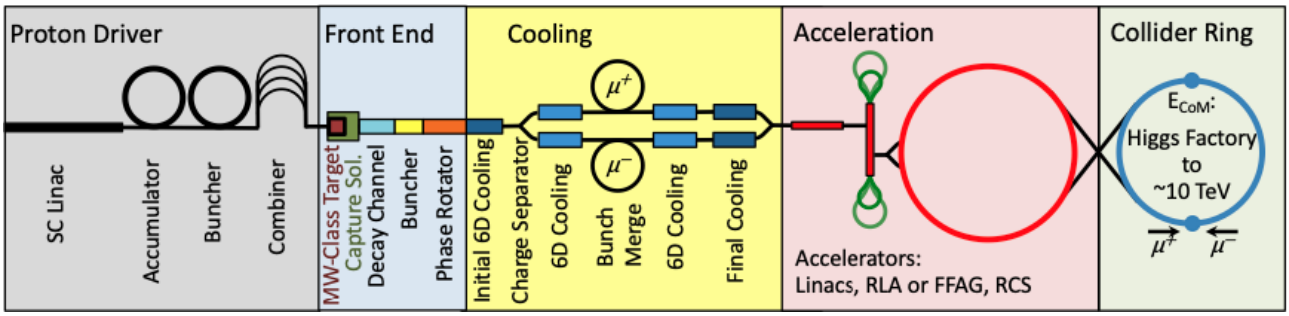

Figure (1.2) *Schematic layout of the considered designs for the muon collider. Adapted from The International Muon Collider Collaboration [4].*

In multiple parts of the muon collider magnetic fields are used, but the most technologically challenging processes are the cooling process and the target and capture process [5]. For cooling the muons, ionization [6] needs to be used as that is the only process that is fast enough to cool the muons before they decay. In this process, the momentum of the muons is reduced while they are focused by a magnetic field. The magnetic field strength has a large influence on the efficiency of the cooling process. Currently, systems designed for this cooling process are based on 30 Tesla solenoids [7], which is a field strength that has been experimentally demonstrated in other applications.

The target and capture process is the application that this report focuses on. The goal of this process is to produce muons. To do this, pions are produced by a short and intense interaction of proton bunches, after which the pions are captured by a high field target solenoid. This magnet also guides the pions into the decay channel, where they decay into muons, among other particles. The muons are captured by a combination of solenoids and radiofrequency (RF) cavities. The requirements for the cable used in this target and capture magnet in a recent design are presented in Tab. 1.1.

Operating current	58 kA
Operating field	20 T
Operating temperature	20 K

Table (1.1) *Requirements cable for target and capture magnet in recent design [8].*

To design a superconducting magnet that fulfils these requirements, multiple aspects need to be studied. The shape and size of the magnet need to be determined, but also the composition and configuration of the cable. A schematic representation of the target and capture magnet is given in Fig. 1.3.

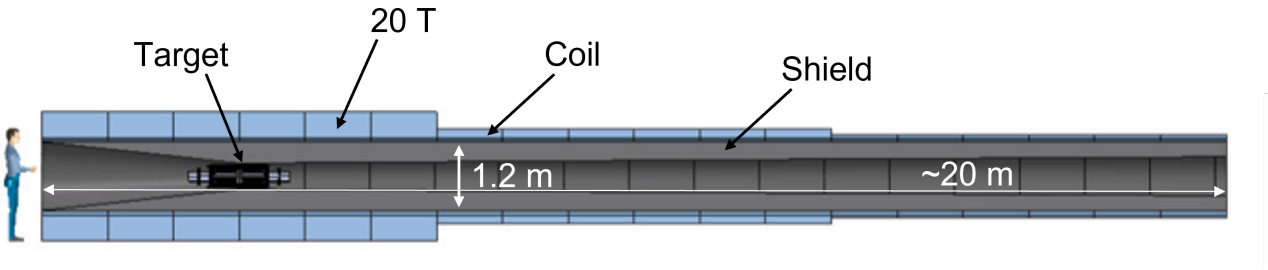

Figure (1.3) *Schematic image of recent design for target and capture magnet. Adapted from L. Bottura et al. [9]*

The shape of the target and capture magnet is a solenoid, which is a helical coil, resulting in a large magnetic field in the centre of the solenoid. The radius of this solenoid needs to be quite large to fit all the required equipment. Currently, a radius of 0.6 m is proposed, which is quite large in comparison to other applications, including the cooling process. When a magnet has a large diameter, the forces on the solenoid are higher as well. More specifically, the hoop stress (σ_θ) is proportional to the magnetic field strength (B), current density (J) and radius (R) of the magnet as described in Eq. 1.1 [10].

$$\sigma_\theta = BJR \tag{1.1}$$

Therefore, the large radius of the target and capture magnet, together with the large operating current and magnetic field, increases the importance of sufficient mechanical strength in the solenoid. This is one of the main challenges of this magnet, but definitely not the only one. Other challenges are for example infrastructure and operating costs.

For both the cooling process and the target and capture process, very high magnetic fields are required and to achieve this, superconductors [11] are used. Superconductors are suitable because, at a certain critical temperature, their resistance drops to zero, while ordinary conductors do have resistance. Even though superconductors do require energy to go to very low temperatures, superconducting magnets require much less power, making them an economical choice.

1.3 Superconductors

There are various types of superconductors, which all have different characteristics. Superconductors can be divided into two categories: low-temperature superconductors (LTS) and high-temperature superconductors (HTS). A superconductor reaches the superconducting state (zero resistance) when it is cooled below its critical temperature (T_c) [12]. If this T_c is 77 K or higher, the superconductor is classified as an HTS. Apart from the critical temperature, there are two other critical parameters that set the range in which a material is in its superconducting state. These are the critical current (I_c) and the critical magnetic field strength (B_c). This operating range, called the critical surface, formed by these parameters is presented in Fig. 1.4. This figure also shows that HTS have a much larger critical surface than LTS, which makes it

suitable for higher field and temperature applications. Especially the T_c above 77 K is a huge advantage, because this is the boiling point of liquid nitrogen, and thus HTS can be cooled using liquid nitrogen (LN_2).

There are several high-temperature superconductors [11]; most of them are ceramic materials, and some are metallic materials. Ceramic materials are often brittle which causes several drawbacks. However, they are still being studied for their exceptionally large operating range. The most common ones are rare-earth barium copper oxide (ReBCO), the most famous one being yttrium barium copper oxide (YBCO).

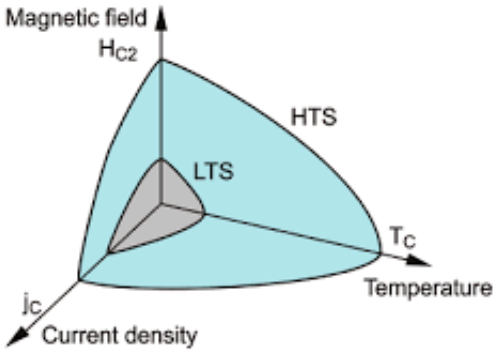

Figure (1.4) *Schematic image of the critical surface of superconductors [12].*

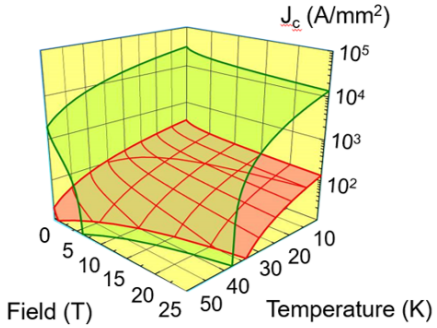

Figure (1.5) *Critical surface of ReBCO by A. Kario [13].*

1.4 ReBCO

The characteristic that makes ReBCO [11] stand out is its potential for applications using stronger magnetic fields than other superconductors. However, ReBCO is a ceramic and thus brittle material. Therefore, it cannot handle the large forces that it has to face in a high field magnet. From ReBCO, tapes are produced, that consist of various different layers encapsulating the ReBCO material. This ensures that the ReBCO material is deposited with crystallographic orientation. More specifically, grains below 5 degrees need to be arranged so that the current crosses the grain boundaries. Grain boundaries with a misalignment of more than 5 degrees have a very low critical current, reaching even 1/50 of the critical current of ReBCO with properly aligned boundaries. To make such an exact alignment of grains a precise manufacturing route needs to be followed, which does not work for the manufacturing of round wires. A schematic of this tape is presented in Fig. 1.6. These tapes are usually 4 mm or 12 mm wide and 0.1 mm thick [14]. The basis is a substrate, which is polished to decrease the possibility of defects in the ReBCO layer. Then there is a layer of buffers, which have similar lattice parameters as the ReBCO material, and thus serve as a base to grow the ReBCO layer. The ReBCO layer is coated with a silver layer as chemical protection. On top of this, a copper layer can be applied as an electrical stabilizer [15].

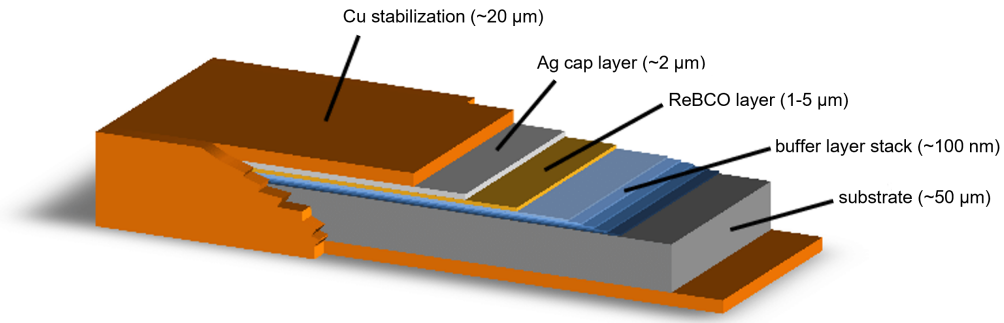

Figure (1.6) *Schematic layout of ReBCO tapes. The image is not up to scale. Image adapted from C. Barth et al. [14].*

ReBCO superconductors have very high potential due to their large critical surface (Fig. 1.5). Namely, for a magnetic field of 18 Tesla at 4.2 K, the critical current ranges between 203 A to 305 A for tapes that are 4-4.8 mm wide [16]. However, the critical current of a ReBCO tape is apart from magnetic field strength and temperature, also dependent on the angle. This is caused by the flat shape of the tape. Therefore, the angle between the tape and the magnetic field is of great importance for the critical current. Adding to this, the mechanical properties are also of great importance. In the muon collider, this material can be used to produce a magnetic field, by running a current through it. Following Fleming's right-hand rule, there will also be a force on the material when there is a current and a magnetic field. The force is called the Lorentz force (F_{L}) [17] and is described in Eq. 1.2.

$$F_L = \vec{J} \times \vec{B}, \tag{1.2}$$

where $\vec{J}$ is the current density and $\vec{B}$ is the magnetic field.

Therefore, the magnitude of the Lorentz force depends on the direction and magnitude of the current density and the magnetic field. Values for the Lorentz force can get up to 1000 kN m^{-1} [18] in the radial direction of the solenoid. Therefore, the Lorentz force puts the mechanical properties of the ReBCO tapes to the test. For example, this force can cause bending and pulling, which can have an effect on the three critical parameters. In the direction along the wire, strains of more than 0.2% can also occur [18]. Apart from the strain caused by the Lorentz force, winding the coil into its solenoid shape introduces bending strain to the tapes as well.

Several studies (e.g. [19] and [20]) of the sensitivity of individual ReBCO tapes to tension, torsion and bending have already been conducted. However, the effect on the critical current is still an active field of research. Also, the study of stacked ReBCO tapes is quite new and thus still requires much data.

There are various types of stacked cables of which some are more advanced than others. The simplest option is to stack multiple tapes onto each other. Afterwards, the cable can be twisted to improve the current distribution [21] but whether this twist is actually causing an advantage is still under discussion. The effect of bending these cables has been studied and for one specific configuration, it showed that bending at a diameter of 140 mm resulted in a critical current degradation of 5.4% [22]. This current degradation should be minimized, and thus there are more designs considered for these stack cables.

An example of a more complex design is the VIPER (Vacuum pressure impregnated, Insulated, Partially transposed, and Roll-formed) cable [18]. A schematic of this VIPER cable is presented in Fig. 1.7. In this design, there are four stacks of ReBCO tapes that are twisted around the cooling channel. This channel is necessary to enter the superconducting state. Using multiple stacks makes it possible to handle larger currents. However, this cable does have a lower current density than the simple stack, because of its large former.

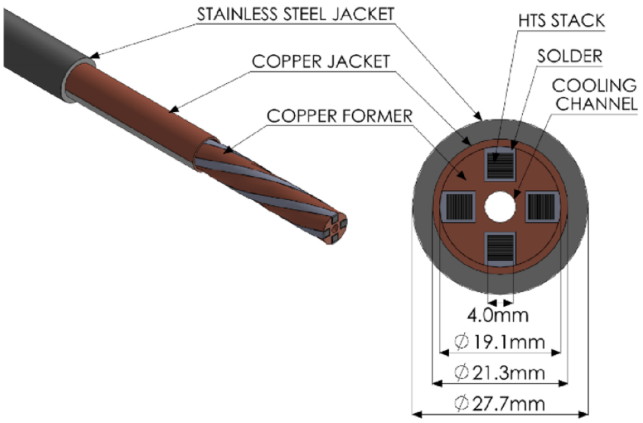

Figure (1.7) *Schematic of the VIPER cable. Image adapted from Fry et al. [18].*

1.5 Assignment

In this study, stack cables, suitable to be incorporated in a cable for the target and capture magnet, based on the ReBCO superconductor will be analyzed using experiments and simulations. More specifically, the effect of bending on the critical current will be studied. First, a literature review is given on the previously performed strain experiments on ReBCO tapes and stack cables together with a strategy to determine the strain theoretically. Next, the stack cable design for this study is motivated in Chapter 3. Following, the theoretical assumptions are confirmed using simulations. In these simulations, the critical current is calculated and the magnetic field is studied while varying the composition of the stack cable. Next, the experimental set-up is discussed in Chapter 4. The experiments are performed in liquid nitrogen to be able to measure the critical current of the ReBCO superconductor. Following, the experimental results are presented and discussed in Chapter 5, leading to an overall conclusion and recommendations in Chapter 6.

2 Literature Review on Bending of ReBCO Tapes and Cables

In this chapter, the theoretical calculations to predict the strain during bending in ReBCO tapes and stack cables are described. Additionally, a review of the previously performed bending experiments on these tapes and stack cables is given.

2.1 Theoretical Strain Estimation

There are theoretical ways to calculate the strain in a ReBCO tape due to bending. Bending can be done in-plane and out-of-plane. Since the tape is asymmetric, as the ReBCO layer is not in the middle of the tape, out-of-plane bending can be done with the ReBCO on the in- or outside. In this study, the tapes are bent with ReBCO on the inside as this leads to more compression than tension in the ReBCO layer and ReBCO can better withstand compression than tension [23]. The difference between in-plane and out-of-plane bending is shown in Fig. 2.1.

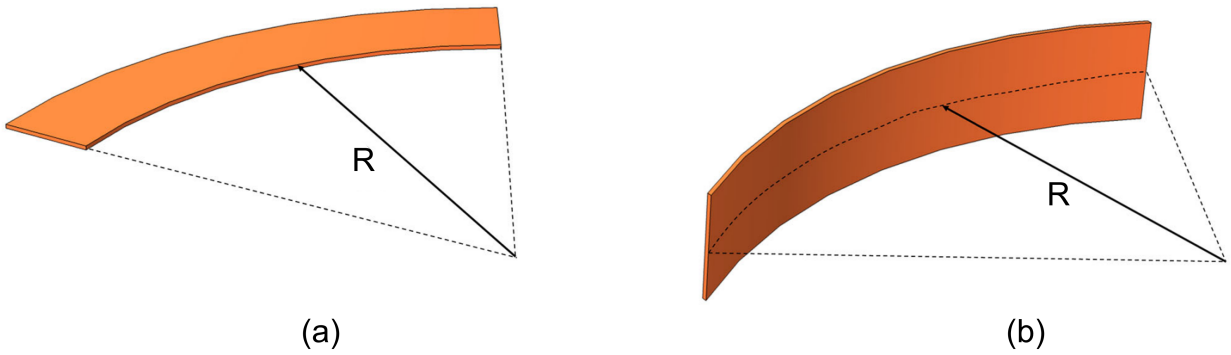

Figure (2.1) *Schematic of a bent ReBCO tape by Pi et al. [24]. (a) in-plane bending. (b) out-of-plane bending.*

To find the strain in the ReBCO, its location in the tape needs to be determined. This is done by finding its distance to the neutral axis, which is in the middle of the sample. It is assumed that this neutral axis stays the same length during the bending. The tapes on the inside of the bend are compressed, while the tapes on the outside are extended. This situation is shown in Fig. 2.2.

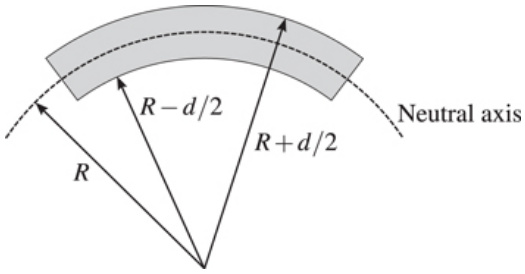

Figure (2.2) *Sketch of the bent sample of thickness d with its neutral axis by Otten et al. [25].*

If y_{n} is the y-coordinate of the neutral axis and y_{REBCO} is the y-coordinate of the ReBCO layer, when the y-axis is perpendicular to the tape, Eq. 2.1 can be used to calculate the strain in the ReBCO layer [24].

$$\epsilon_{\mathrm{Bending}} = \frac{y_{\mathrm{REBCO}} - y_{\mathrm{n}}}{R} \tag{2.1}$$

where R is the bending radius.

This formula has been confirmed to be a good estimation for single tapes but not yet for stack cables. This report will study whether this theoretical estimation suffices for stack cables as well. For a stack, it is

assumed that the tapes are soldered to each other and there is no sliding between the tapes so the stack is bent as a whole. This way, the thickness of the whole stack can be used in the calculations. The neutral axis is assumed to be in the middle of the stack, as shown in Fig. 2.3. In this figure, the silver layer is neglected because it is a relatively thin layer and therefore does not have a large effect on the position of the ReBCO layer in relation to the neutral axis. The strain is calculated by taking the distance from the neutral axis to the ReBCO layer. The outer ReBCO tape experiences the most tension so this tape will probably break the fastest.

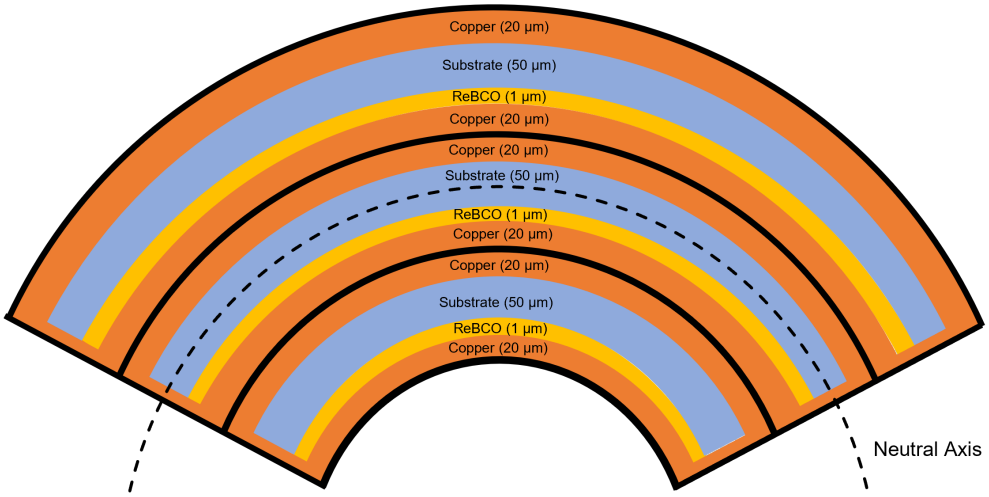

Figure (2.3) *Sketch of bent ReBCO stack of three tapes with its neutral axis. The thicknesses of the layers are an approximation and not drawn to scale.*

2.2 Experimental Data for Strain Limits of ReBCO tapes

When the strain has been calculated, it is important to know which strains are of interest. The strain limits of single ReBCO tapes have been studied multiple times (e.g. [19], [26] and [27]). These limits can be used as an estimate and comparison for the strain limits of the stack cable, which is studied in this report. Therefore, the strain experiments that have been performed on single ReBCO tapes are summarized below. Since the substrate layer is the thickest layer in a ReBCO tape, it is expected that this layer has the largest effect on the critical bending radius ($\sim$5% critical current degradation). In this section, pulling and bending experiments are discussed. In the bending experiments, the ReBCO tapes are bend out-of-plane, with the ReBCO on the outside (see Fig. 2.1) resulting in tension to the ReBCO layer.

Van der Laan et al. [19] tested YBCO-coated conductors from SuperPower with a 50 µm thick Hastelloy substrate. Strain was applied by bending a CuBe spring on which the ReBCO tape sample was mechanically fixed by soldering. They found that 0.5% bending strain resulted in 13% critical current degradation at 77 K, self-field.

Shi et al. [26] bent ReBCO tapes around cylinders with various diameters. They tested three different copper laminated ReBCO tapes manufactured by Fujikura, Shanghai Superconductor and Samri Advanced Materials. For the first two tapes, which have a substrate thickness of 50 µm, the degradation was below 5% for a bending radius of 5 mm. However, the third tape, with a substrate thickness of 60 µm, experienced a 10% degradation at a radius of 7 mm. Therefore, in this test, a thicker substrate has a negative effect on the critical current degradation by bending.

A similar result was found by He et al. [28] who tested the ReBCO tapes of SuperPower, Samri Advanced Materials and Shanghai Superconductor. These tapes have a substrate thickness of 50, 60 and 35 µm respectively. In this study, the strain limit of ReBCO tapes was investigated by bending the tapes around hollow epoxy cylinders and by applying uniaxial tension. The study showed that the SuperPower tapes were the most flexible with a 5% I_c degradation with a bending radius of 4.5-5.15 mm. In comparison,

the critical radius of Samri tape was found to be 7-7.5 mm. For these two tapes, the statement that a thicker substrate leads to a larger critical radius holds. However, the Shanghai tape had a critical radius of 6-6.5 mm despite the thin substrate layer. Therefore, it is assumed that there is an optimal thickness of the substrate layer that is about 50 µm. This study also showed that the irreversible strain limit for the three different ReBCO tapes was between 0.28% and 0.57%. Again, the SuperPower tape showed the best results (0.5-0.57%), but for this limit, the Shanghai tape showed the worst results (0.285-0.3%).

Zhou et al. [27] performed various stress-strain experiments on five different ReBCO tapes with different substrate thickness: AMSC (50-75 µm), Bruker (97 µm), Fujikura (100 µm), SuNAM (60 µm) and SuperPower (50 µm). The ReBCO tapes were fixed to a U-shaped spring, which was bent to apply strain to the tapes. This experiment showed that the tapes showed a small I_c degradation before reaching the irreversibility limit. This irreversibility limit was between 0.28% and 0.6% for the different tapes and the SuNAM tape showed the best results. The AMSC tape showed the worst results, but this tape contains Ni-5W substrate instead of Hastelloy which is used in most tapes. Therefore, Hastelloy seems to be the best substrate type to use, but stainless steel (SS) substrate is also suitable as the Bruker tape shows good results with an irreversibility limit of 0.4%.

Barth et al. [14] studied the irreversible strain limits of ReBCO tapes by soldering them to a Walters spring probe. This spring has a helical shape around which the ReBCO tape is wound. The wounds have different radii in order to find the critical bending radius. This study included five different ReBCO tapes, of which Fujikura (75 µm) and SuperOx (60 µm) have not been discussed yet. For these tapes, the Fujikura tape had a better irreversible strain limit than the SuperOx tape. Also, for the three other tapes that they tested (Bruker, SuNAM and SuperPower) they found better results than the previously discussed studies found. Comparing all the different tapes in the study, Bruker showed the best irreversible strain limit of 0.70%-0.72%.

All results are summarized in Tab. 2.1. Interestingly, even though the experiments used different strategies to measure strain limits, the results are all in the same range. From the results can be seen that the irreversible strain limit is on average higher for tapes with a thicker substrate layer. Additionally, for most tapes, the first critical current degradation can be seen at about 0.4% strain, but it is still reversible, while at 1.0% strain it is sure that the tape has been irreversibly damaged. These two limits are studied during the experiments. When looking at the critical bending radius, it is the smallest for tapes with a substrate thickness of 50 µm, but this has not been researched for all the different available tapes.

Tapes	Substrate Type	Substrate Thickness	Critical Bending Radius	Irreversible Strain Limit
SuperPower	Hastelloy	50 µm	4.5-5.15 mm	0.41-0.69%
Fujikura (50 µm)	Hastelloy	50 µm	5 mm	-
Shanghai (50 µm)	Hastelloy	50 µm	5 mm	-
Samri	Hastelloy	60 µm	7-8 mm	0.4-0.43%
Shanghai (35 µm)	Hastelloy	35 µm	6-6.5 mm	0.285-0.3%
AMSC	Ni-5W	50-75 µm	-	0.28%
Bruker	SS	97 µm	-	0.4-0.72%
Fujikura (100 µm)	Hastelloy	100 µm	-	0.4%
SuNAM	Hastelloy	60 µm	-	0.6-0.68%
Fujikura (75 µm)	Hastelloy	75 µm	-	0.56-0.58%
SuperOx	Hastelloy	60 µm	-	0.47-0.49%

Table (2.1) *Summary of the experimentally tested bending parameters of ReBCO tapes [14], [26], [27], [28].*

2.3 Bending Experiments on ReBCO Cables

A few ReBCO cables have been studied as a function of bending radius. The flexibility of cable depends highly on the composition of the cable. Some ReBCO cables are built around a former, such as the VIPER cable that was discussed in Ch. 1. This increases the strength of the cable, but also makes it stiffer. In this section, the critical current degradation caused by bending of a few ReBCO cables is discussed.

First of all, the ENEA cable has been studied, which has a similar design as the VIPER cable but it consists of five stacks. The experiment on the ENEA cable showed that at a bending radius smaller than 250 mm there was severe critical current degradation (4-10%) [29].

Also, the quasi-round stack cable showed an I_c degradation of 5% at 0.54% bending strain, at a bending radius of about 500 m [30]. This cable consists of a single stack, with some protection in the form of copper wires and tin solder around it. Another experiment on this type of cable showed an I_c degradation of 5% at a bending radius of 350 m [31].

Another cable that has been tested is the CERN Aluminium-Stabilized HTS cable [32]. This cable is made up of a single stack that is soldered after which it is put inside an aluminium stabilizer. The experiment performed with two samples of this cable used a bending radius of 100 mm which caused failure of the cable. One sample consisted of six tapes and the other cable of seven tapes. Therefore, they advise using a radius larger than 250 mm.

The discussed results for the bending experiments on stack cables are summarized in Tab. 2.2. The study of Shi et al. [30] matches well with the irreversibility limits of the single ReBCO tapes. The bending radii of interest for stack cables lie between 250 and 500 mm, but this depends on the thickness of the stack (Eq. 2.1).

Cables	Critical Bending Radius
ENEA	250 mm
Quasi-round	350-500 mm
CERN AS	$\sim$250 mm

Table (2.2) *Summary of the experimentally tested critical bending radii of ReBCO cables [29]-[32]*

3 Stack Cable Design

Designing a superconducting magnet is a complex task, as the critical current of a superconductor is dependent on the temperature, magnetic field and, in the case of ReBCO tapes, tape orientation. This section explains the design choices for the ReBCO based stack cable. These design choices are based on calculations and literature research, using the available material. The material properties of the used tape are discussed and these are linked to the requirements of the target and capture magnet. The critical current and magnetic field of the designed cable are estimated using a Matlab simulation.

3.1 SuperOx ReBCO Tape

The ReBCO tape that is used in this study is the SuperOx - 4 mm, 63 µm Hastelloy. The specifications of this tape are presented in Tab. 3.1.

Substrate	Hastelloy C276
Thickness substrate	$63 \pm 3\,\mu\mathrm{m}$
Width substrate	$4 \pm 0.13\,\mathrm{mm}$
Silver layer HTS side	$2 \pm 0.5\,\mu\mathrm{m}$
Silver layer substrate side	$1 \pm 0.5\,\mu\mathrm{m}$
Copper layer	$20 \pm 4\,\mu\mathrm{m}$ per side
Solder plating, InSn eutectic	$5{-}10\,\mu\mathrm{m}$ per side
Min. I_c (77 K, s.f.)	$<150\,\mathrm{A}$
Lift-factor at $4.2\,\mathrm{K}$, $1\,\mathrm{T}$ $(B//c)$	5.8
Expected I_c at $4.2\,\mathrm{K}$, $1\,\mathrm{T}$ $(B//c)$	< 1000

Table (3.1) *Specifications of the SuperOx tape.*

This tape can operate at a field of 20 T and at a temperature of 20 K, but the critical current has not been measured under these exact circumstances yet. However, a study reaching 20 K and 19 T on another 4 mm SuperOx tape has been performed by Senatore et al. [33]. The results from this experiment are presented in Fig. 3.1.

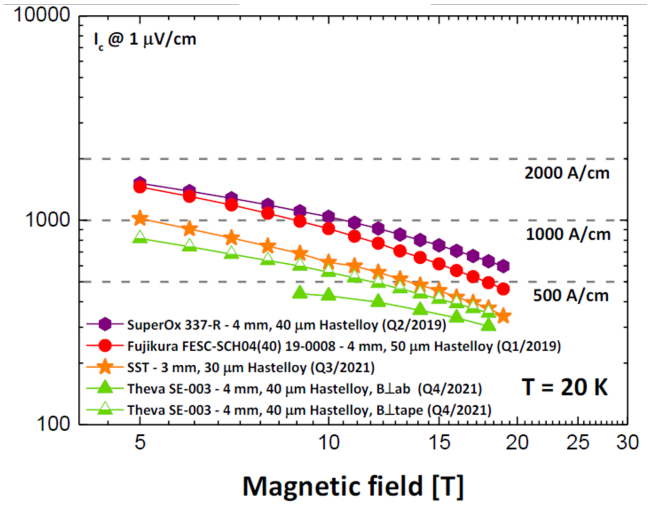

Figure (3.1) *Behaviour of various tapes at* $20\,\mathrm{K}$ *under different magnetic fields measured by Senatore et al. [33].*

From the graph presented in Fig. 3.1 it can be estimated that the critical current density at 20 K and 20 T is about 550 A cm^{-1}. This leads to a critical current of about 220 A. Taking into account that the operating current should be 58 kA to fulfil the requirements of the target and capture magnet, this means

that more than 260 tapes with a width of 4 mm in a cable structure are required to build a suitable magnet. As this is not in the scope of this project, different smaller samples are tested in a one-stack design and from that the trend will be studied to be able to conclude on the behaviour when upscaled. Additionally, these single stacks could be implemented in a multi-stack cable, such as the VIPER cable.

3.2 Strain Calculations

Therefore, stacks of 5 and 10 tapes are chosen to find the trend in the critical current degradation with the amount of tapes in the stack. These values are chosen to clearly understand the physics of the stack cable. When this behaviour is understood a full cable design with hundreds of tapes can be studied. Two different sample sizes are required to find the dependence on the amount of tapes of the bending limit. In this part, the strain limits are calculated.

As mentioned in Ch. 2, at 0.4% strain ReBCO tapes experience critical current degradation and at 1.0% strain the ReBCO tape will certainly break. These two limits are calculated for the two different stacks using Eq. 2.1 [25]. It is assumed that the tapes are soldered together and that the stack bends as a whole. The limits, calculated for the outermost tape which experiences the most tension, are presented in Fig. 3.2.

From these limits is decided to bend the cables at a radius of 250, 150 and 50 mm. These points are marked in Fig. 3.2, from which can be seen that for both samples the expected 0.4% bending strain will be reached and for the stack with 10 tapes the 1.0% bending strain will be reached as well. With these measurements, it is expected that a clear image of the critical current degradation of the different stack cables is established.

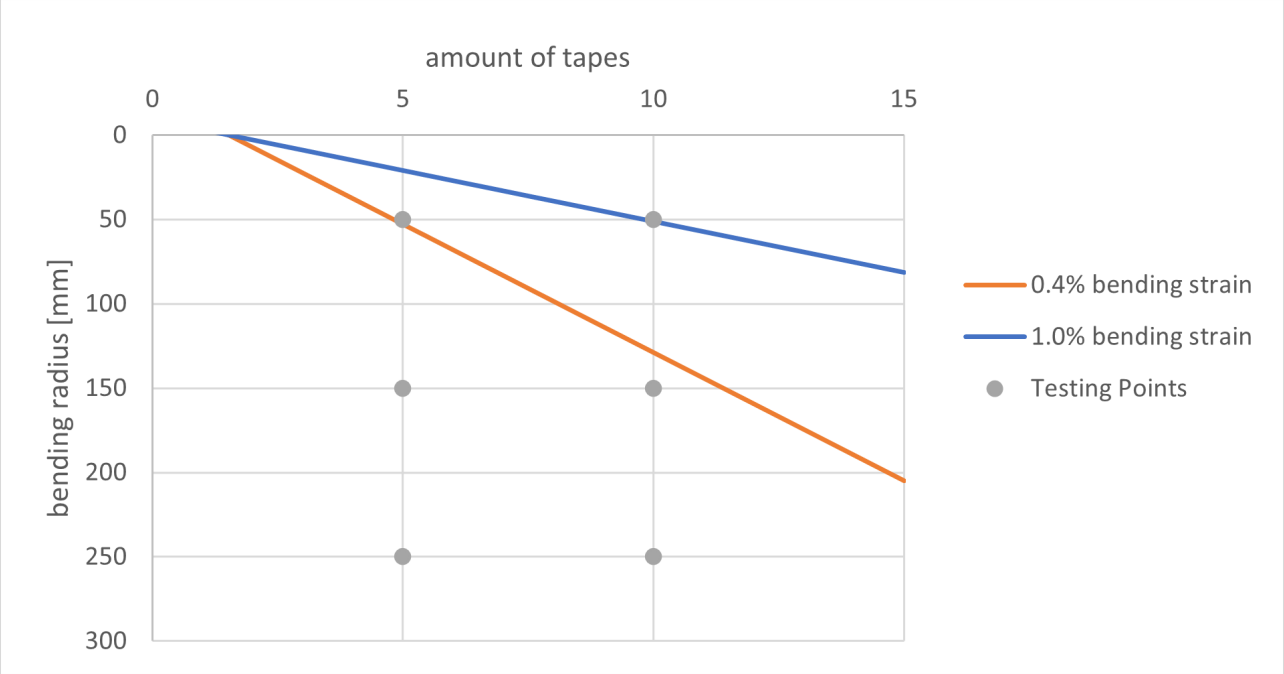

Figure (3.2) *Bending radius at which the calculated bending strain in the outermost ReBCO layer of the stack reaches 0.4 and 1.0%, including the chosen testing points. In these calculations, it is considered that the ReBCO layer is on the inward-facing side of the substrate.*

3.3 Critical Current Simulations

Before performing the experiments, the effect of the self-field of the stack cables is studied in a Matlab simulation. Self-field is the magnetic field that is created by the current flowing through the tapes. The magnetic field of each tape interferes with the magnetic field of the other tapes, which reduces the current

through these other tapes. In this simulation, the magnetic field and the critical current are studied, while varying the amount of tapes in the stack and the distance between these tapes.

3.3.1 Matlab Simulation

In the Matlab simulation, the critical current and the magnetic field behaviour are calculated. This is done by splitting the tapes into elements and iteratively calculating the current distribution that satisfies $J{=}J_{\mathrm{c}}(B{,}\theta)$ in all elements. J_{c} is the local critical density in A/m, which depends on the magnetic field strength (B) and the angle between the magnetic field and the tape normal (θ). The critical current of the stack is found by integrating the critical current density over all the elements and all the tapes. It is important to split the tape into elements because the direction and magnitude of the magnetic field is different along the width of the tape. The amount of elements can be chosen, depending on what accuracy is desired. For the simulations performed in this study, the amount of elements per tape is set at 20. There are a few more input parameters, which are the width of the tape, the distance between the tapes and the number of tapes in the stack. The width is set to 4 mm, the width of the used SuperOx tape, and the other two parameters are varied. The amount of tapes is studied to estimate the self-field effect in relation to the amount of tapes, which will be compared to the experimental results. The effect of the tape separation on the critical current is simulated to comment on the influence of the thickness of the tape and solder between the tapes. The simulation uses experimental critical current data dependent on the angle and magnetic field from a similar SuperOx tape that is scaled to match the used SuperOx tape [34]. The experimental data is achieved under self-field conditions at 77 K. The critical current of a single tape is 114 A, which was found experimentally as can be read in Ch. 5.

3.3.2 Amount of Tapes

In the experiment, two different cables are studied, which consist of 5 and 10 tapes. In general, doubling the amount of tapes means that the critical current doubles as well. However, due to the magnetic fields of the different tapes interfering with each other, this relation does not hold and the critical current is influenced by the self-field. Fig. 3.3 shows that the I_{c} of a stack of 5 tapes is 463 A but the I_{c} of a stack of 10 tapes is 798 A.

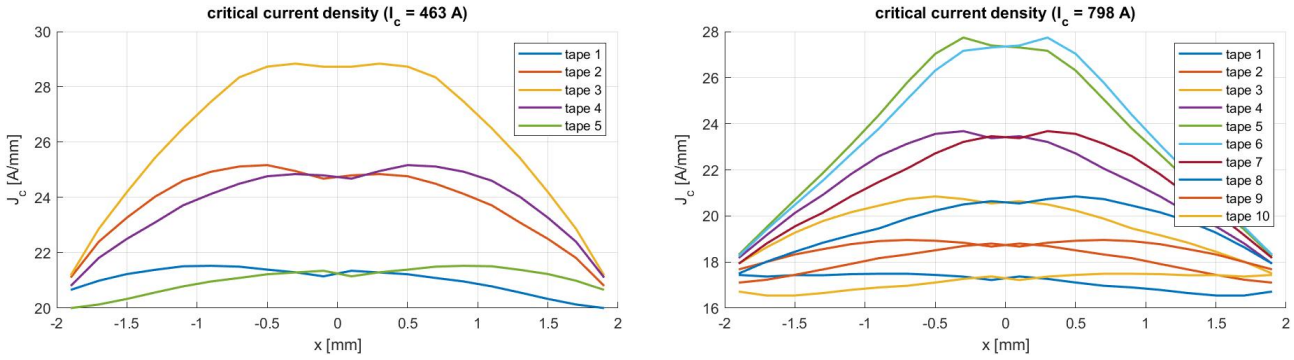

(a) *5 tapes* **(b)** *10 tapes*

Figure (3.3) *Graphs of the local critical current density against the location along the width of the tape showing the effect of stacking tapes on the critical current.*

3.3.3 Distance between Tapes

The distance between the tapes also has an effect on the critical current of the stack cable. When the distance is larger, the tapes interfere less with each other, which results in a higher critical current. Therefore, the thickness of the tape and the solder between the tapes can have an effect on the critical current.

This effect is presented in Fig. 3.4 for a stack with 10 tapes. Since the solder can have a thickness of the order of 100 µm this can result in a difference in I_c in the order of 100 A for a stack of 10 tapes.

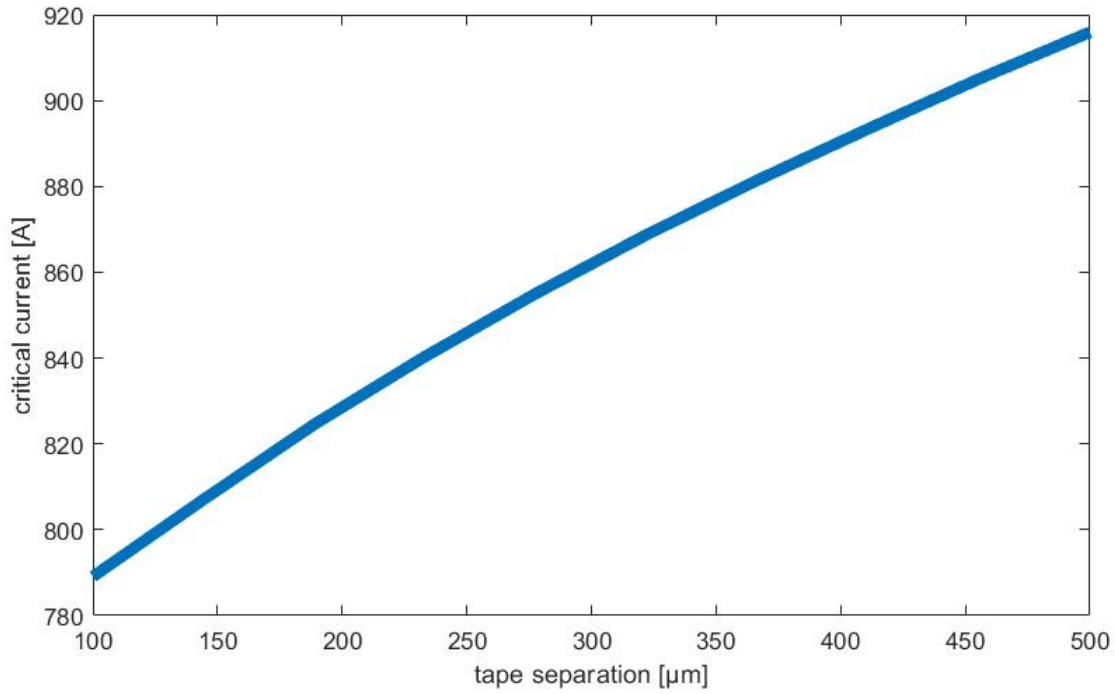

Figure (3.4) *The effect of separation between ReBCO layers on the critical current for a stack cable with 10 tapes.*

4 Bending Measurement Set-Up

In this chapter, the experimental methods are explained. The experimental methods contain the preparation of the stack cable and the experimental set-up for measurement of the effect of bending on the critical current.

4.1 Sample Preparation

To produce a soldered stack, the ReBCO tape is cut into pieces of 507 mm. Of this 507 mm, 157 mm is bent, 300 mm is used for the current contacts and the other 50 mm is used as a buffer and to connect the voltage taps to. The tapes are all a slightly different length to create an equally spaced staircase connection in the current contacts. As solder, InSn ribbons are used, which are made by rolling a round wire. Afterwards, they are cleaned with isopropanol, to ensure that there is no grease on the surface. The stacks are made using a soldering tool that is shown in Fig. 4.1. This soldering tool was designed by us and manufactured at the University of Twente. The soldering tool is made up of aluminium, due to its high thermal conductivity. Additionally, the InSn solder does not wet aluminium so the sample can be removed easily. The tapes are placed inside the groove with an InSn solder ribbon between each of the tapes. Flux is applied to the tapes to remove metal-oxide layers which hinder soldering on the ribbons. Then the upper part of the tool is pushed onto the tapes using springs with a pressure of 1.5 MPa and the entire device is heated to 140 degrees Celsius for two hours in an oven to melt the solder. The stack is compressed and forms a solid cable. The excess solder is also pushed out of the stack during this process. After the tool and stack are cooled down, the lid and the sides of the tool are removed, to take out the stack without damaging it.

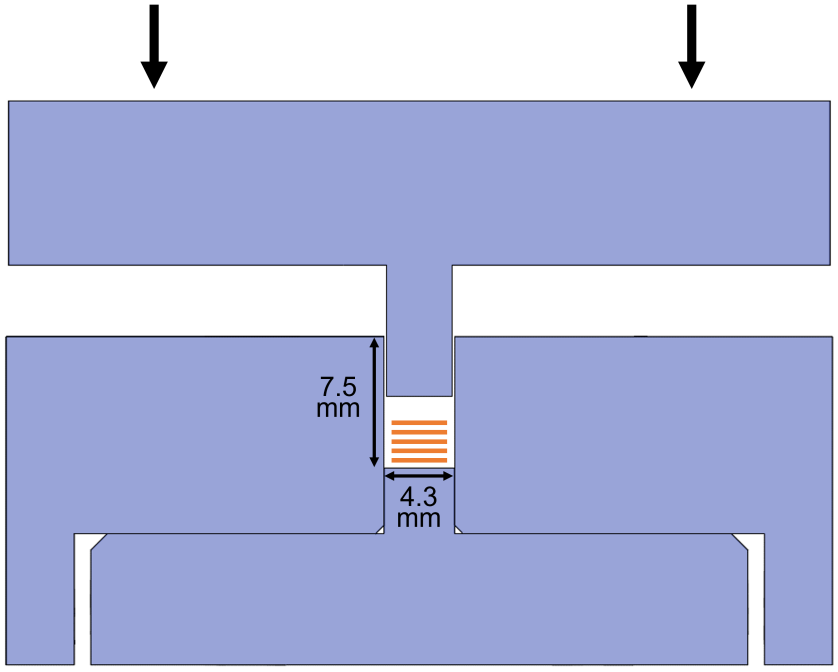

Figure (4.1) *Schematic image of tool for stack soldering, including the stack (orange). The arrows represent the force that is applied using springs.*

4.2 Testing Set-Up

After the soldering process, the current leads are clamped to the ends of the cable. The tapes on each end of the cable are cut into a staircase form. These staircases of a length of 150 mm on both ends are inserted into copper terminals and clamped with In, to ensure a sufficient connection with all the different tapes.

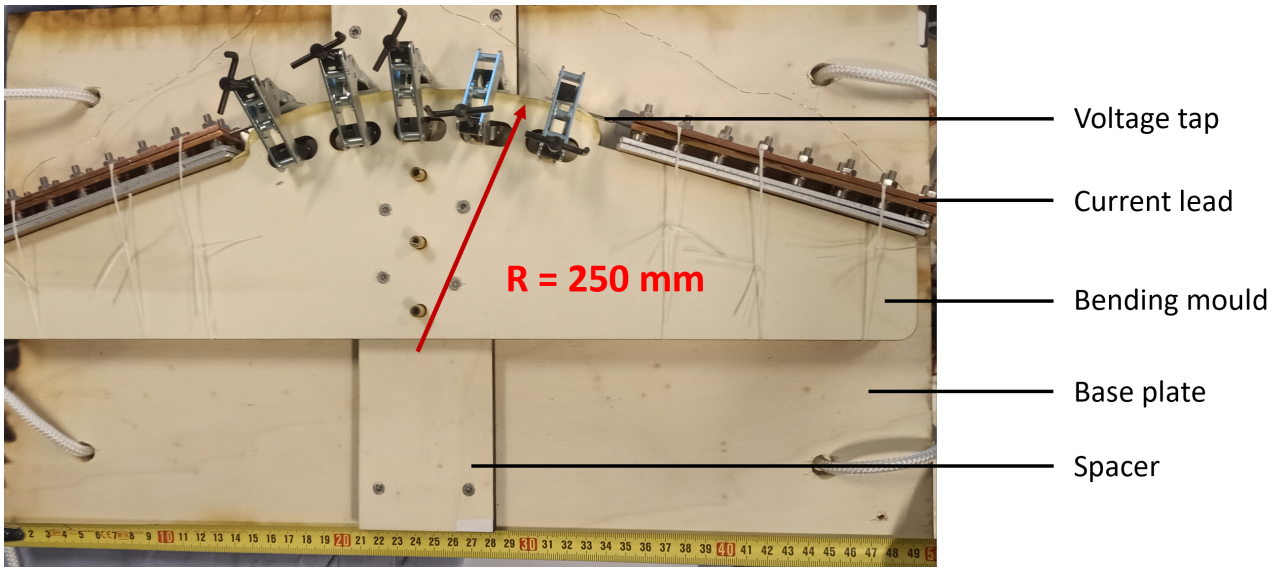

Figure (4.2) *Picture of testing set-up for R=250 mm including the bending mould, spacer, base plate and current leads.*

To bend the cable appropriately, a base plate is constructed for this study, which is presented in Fig. 4.2. On this base plate, the spacer and the wanted bending mould can be attached. These bending plates have an arched part at a radius of 250, 150 and 50 mm. The arched parts are of the same length for the three different plates. The plates contain holes to clamp the cables to bend them at the wanted radius and ensure that the cable forms a round arch. All the plates are made of plywood and are cut using a CO2 laser cutter. This procedure makes it possible to create precise shapes and the material can withstand liquid nitrogen. The voltage taps are attached to the current leads and to the arched part of the sample and the entire set-up is put inside a liquid nitrogen bath. The measurements are performed at $77\,\mathrm{K}$ at self-field (s.f.). Therefore, the expected maximum critical current is $150\,\mathrm{A}$ per tape (see Tab. 3.1), which leads to a total maximum critical current of $1500\,\mathrm{A}$ for the stack with 10 tapes. However, when taking the effect of the self-field into account, the critical current is expected to be about $900\,\mathrm{A}$ for the stack with 10 tapes. Thus, the current leads are designed for this critical current with some buffer to avoid overheating the current leads. They are 150 mm long on each side and made of copper to ensure a good electrical connection.

4.3 Critical Current Measurements

To measure the critical current, a voltage-current (VI) measurement is done. The necessary equipment is assembled on a stand. This contains three small current sources (Power Supply SM 15-200 D - Delta Elektronika), one large current source (Programmable DC Power Supply MSD5-4500/415 - Magna-Power), a nanovolt meter (Sensitive Digital Voltmeter Model 182 - Keithley) and a quench detector (DC Quench Detector - Moekotte Automatisering). The measurement starts by gradually increasing the current using a current source and the voltage is measured with a nanovolt meter for each increment. To avoid burning the superconducting cable, a quench detector is used that shuts the power off when it measures a few millivolts of voltage. From the VI-curve, the critical current and the n-value can be determined. The critical current can be found at the critical voltage (V_c), which is set by the critical electric field (E_c) of 1 µV cm^{-1}. The n-value describes the slope of the change from superconducting to general conducting in the VI curve. HTS usually have an n-value between 20 and 40, while a non-superconducting material has an n-value of 1. Inhomogenous or damaged superconducting samples usually have a lower n-value than homogeneous samples. The n-value is determined by fitting Eq. 4.1 to the measured VI curve.

$$\left(\frac{V}{V_c}\right) = \left(\frac{I}{I_c}\right)^n \tag{4.1}$$

By taking the natural logarithm of both sides and rewriting the formula the relation is such that n is the slope of the graph and the I_c can be derived from the y-intercept, as shown in Eq. 4.2.

$$\ln\left(\frac{V}{V_c}\right) = n\ln(I) - n\ln(I_c) \tag{4.2}$$

In the determination of the n-value, the part of the experimentally achieved VI curve is used where the voltage is higher than $V_c/5$. This is the part of the graph where the sample changes from superconducting to normal conducting.

5 Results and Dicussion

5.1 Single Tape

First, a VI measurement of a single tape was performed. The VI curve, presented in Fig. 5.1, shows that the critical current is 114 A. The offset of 7.5 µV is removed from the data. This critical current is inside the expected range of 89 to 149 A, but below the average I_c of 132 A. These are values measuered by the manufacturer as presented in Tab. 3.1. The measured critical current of 114 A is used in the simulations in Ch. 3. The n-value of 33 also shows that this is a homogeneous superconductor. The derivation of the n-value is shown in Fig. 5.2. The errors in this data are too small to show in the figures, apart from the error in the critical voltage ($\pm$ 0.5 µV) which is determined by the distance between the voltage taps.

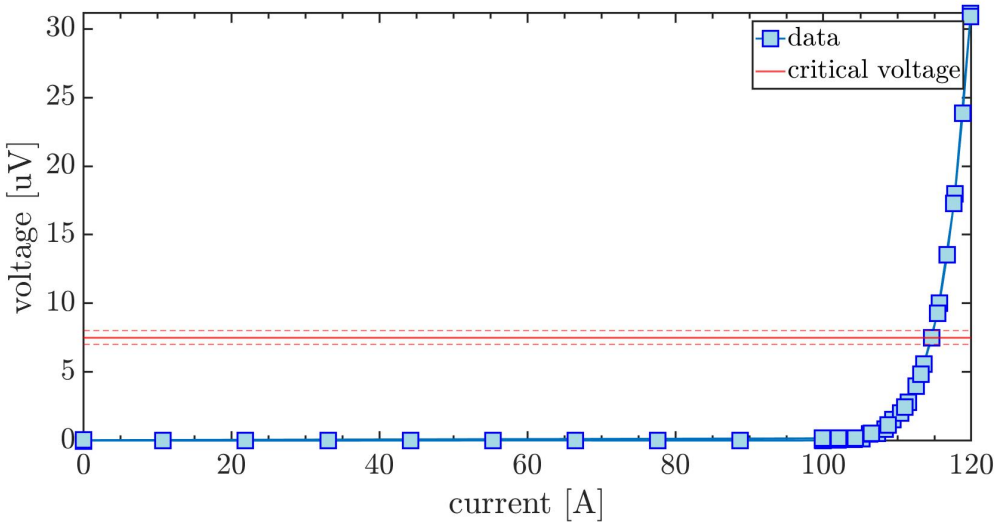

Figure (5.1) *VI measurement of one SuperOx ReBCO tape. On the x-axis, the current is given in Amps and on the y-axis the voltage over the arched part of the cable is given in microvolts. The error of the voltage and current is too small to show in the figure, but the error of the distance between the voltage taps is given by the dashed red lines.*

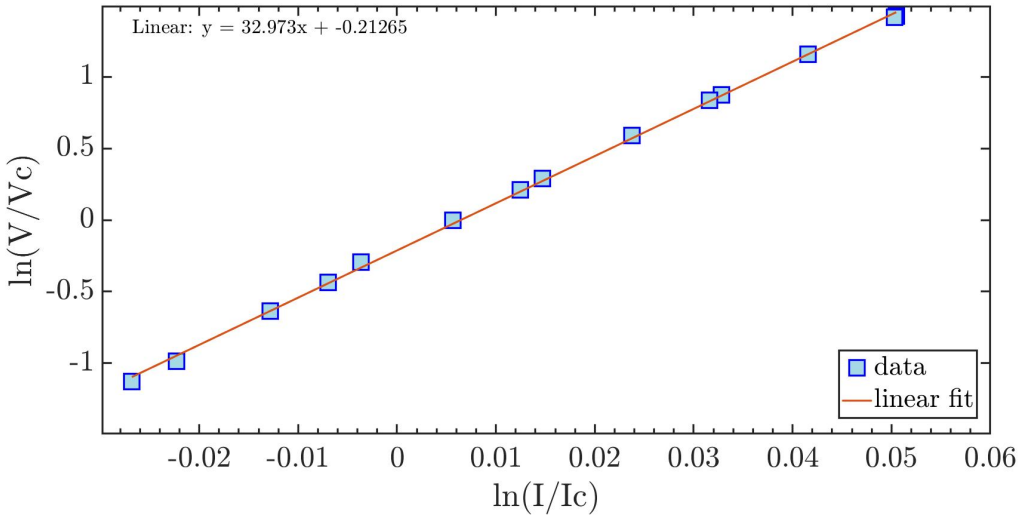

Figure (5.2) *Linear fit of log-log plot of the normalized VI curve. n-value is determined by the slope of the fit.*

5.2 5-tape Stack

The 5-tape stack was put inside the soldering tool and heated up. When it was taken out of the tool, there were gaps between the tapes and some tapes completely separated from each other. This could be caused by the lack of cleaning the tapes before soldering them, which led to a repetition of the soldering process before which the cable was put into a bath of isopropanol and flux was applied between the tapes. After soldering for the second time, the solder was distributed equally and had a thickness of 100 to 200 µm along the cable.

Fig. 5.3 presents the VI curves for the 5-tape stack. The critical currents and n-values are given in Tab. 5.1. The critical current of the straight stack is slightly higher than the 463 A that the simulation calculated (see Ch. 3). For both the radius of 250 mm and 150 mm there is slight critical current degradation, but the n-value stays very high. When the stack was bent to the radius of 50 mm it was expected that it would experience some critical current degradation but 90% degradation is quite severe.

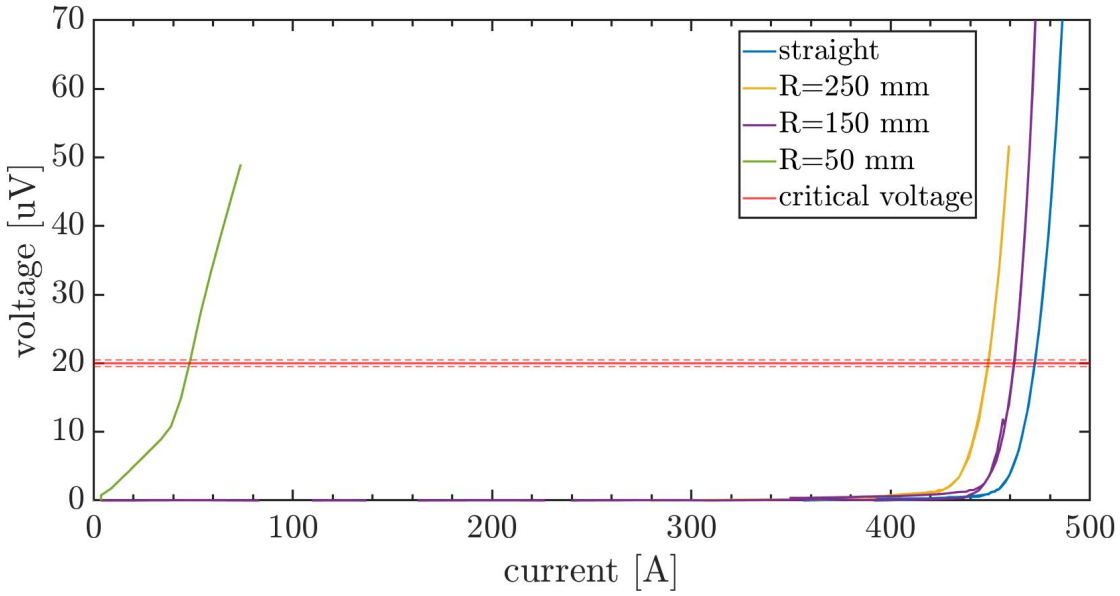

Figure (5.3) *VI curves of 5-tape stack for different radii showing the critical current for each bending radii.*

Radius	Critical Current	n-value	Degradation
Straight	473 A	45	0%
250 mm	449 A	47	5%
150 mm	462 A	56	2%
50 mm	49 A	1.8	90%

Table (5.1) *Critical current and n-value for 5 tape stack dependent on bending radius.*

The weak part of the 5-tape stack was the solder between the tapes. At different parts of the cable, the different layers separated from each other after bending the cable to 50 mm. This can be caused by the fact that the stack had to be soldered twice. In Fig. 5.4 the damage to the cable after bending it at a radius of 50 mm is shown. Fig. 5.4a is at the voltage tap at the edge of the arched part of the cable. This is a weak part of the cable as it is not supported by the bending mould and it is also not inside the copper current leads. Fig. 5.4b shows a part of the arched part of the cable. Here, it clearly shows that bending the cable caused detachment at the soldered interfaces and the inner tapes are buckled to get rid of their extra length. This resulted in extra bending of the tapes at even smaller radii than that of the bending mould, which could have caused more damage and critical current degradation.

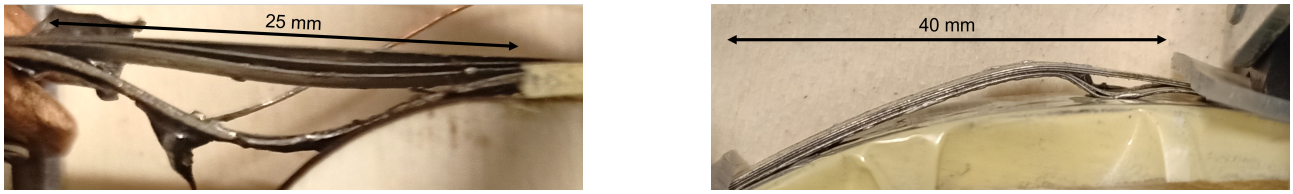

(a) *voltage tap* **(b)** *arched part*

Figure (5.4) *Visible damage to 5-tape stack after bending the cable at a radius of 50 mm.*

5.3 10-tape Stack

Before putting the 10-tape stack in the soldering tool, all the tapes and soldering ribbons were cleaned with isopropanol. Additionally, flux was applied to each of the tapes while stacking them in the soldering tool. The cable was heated in the oven and a solid cable came out of the soldering tool. The solder was also distributed equally with a total solder thickness of 100 to 200 µm along the cable. Only in the middle part of the stack there was less solder (total of 30 µm thickness).

Fig. 5.5 shows the VI-curves for the 10-tape stack and the results are summarized in Tab. 5.2. From the results can immediately be seen that there is much more noise than in the data of the 5-tape stack. This is caused by the large current source, while for the 5-tape stack, three smaller current sources were used. The critical current of the straight cable is 805 A, which is very close to the 798 A that was calculated in Ch. 3. Therefore the stack has not been damaged during the soldering process. However, the n-value was significantly lower than the n-value of a single tape. It was expected that bending at a radius of 250 mm would not result in damage to the 10-tape stack, but the critical current decreased by 20%. Additionally, the n-value decreased much, showing that there is some damage in the sample. This can be caused by bending the cable, but could also be caused by moving the cable during the preparations. When the cable was bent at a radius of 150 mm, the critical current degraded slightly more. This follows the expectations based on the critical strain calculations. When bending at a radius of 50 mm, the cable completely broke and behaved as a normal conductor, which was as expected. However, the mechanism that caused the critical current degradation is different than expected. It was assumed that the stack would bend as a whole and that there would be no sliding between the tapes. This would lead to high tensile strain and degradation in the outer tape. In the experiment, failure of the soldered bond was seen and the inner tapes buckled as shown in Fig. 5.6.

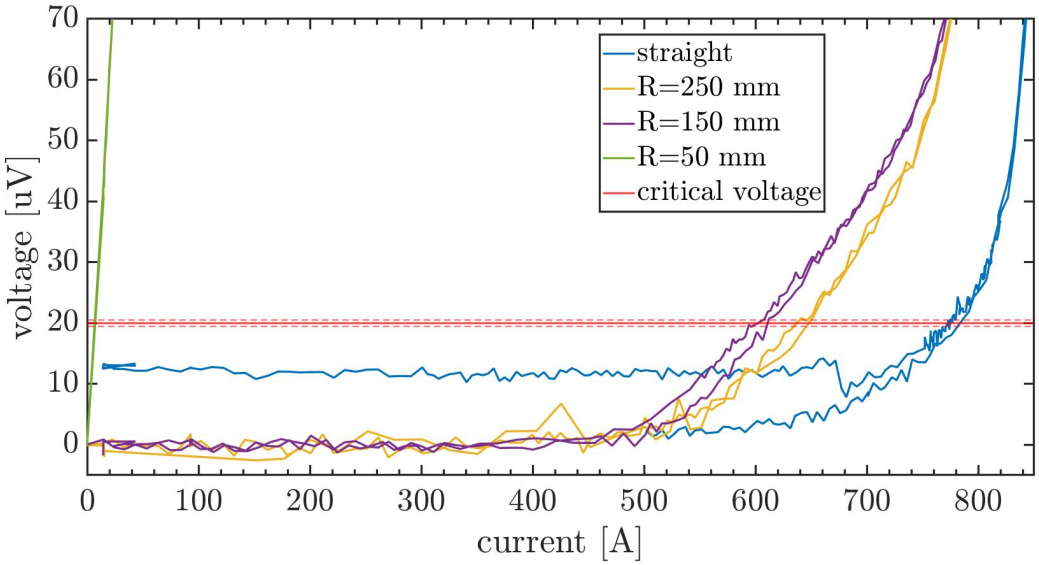

Figure (5.5) *VI curves of 10-tape stack for different radii showing the critical current for each bending radii.*

Radius	Critical Current	n-value	Degradation
Straight	805 A	12	0%
250 mm	645 A	6.9	20%
150 mm	605 A	5.9	25%
50 mm	7 A	1.2	99%

Table (5.2) *Critical current and n-value for 10-tape stack dependent on bending radius.*

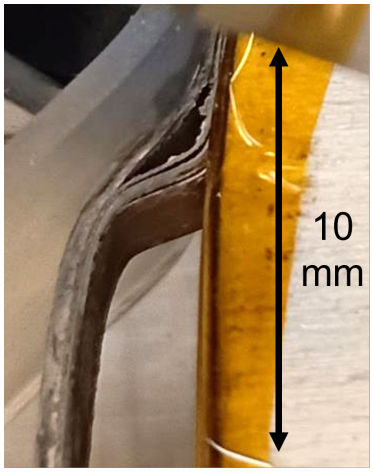

Figure (5.6) *Damage to the 10-tape stack after bending it at a radius of 50 mm.*

5.4 Comparison

In Fig. 5.7 a comparison between the degradation of the 5-tape stack and 10-tape stack is made. From this figure can be seen that the 10-tape stack experienced much more critical current degradation than the 5-tape stack for the radii of 250 mm and 150 mm. For the radius of 50 mm, both cables were broken but for the 5-tape stack 10% of the critical current remained, while for the 10-tape stack only 1% of the critical current remained.

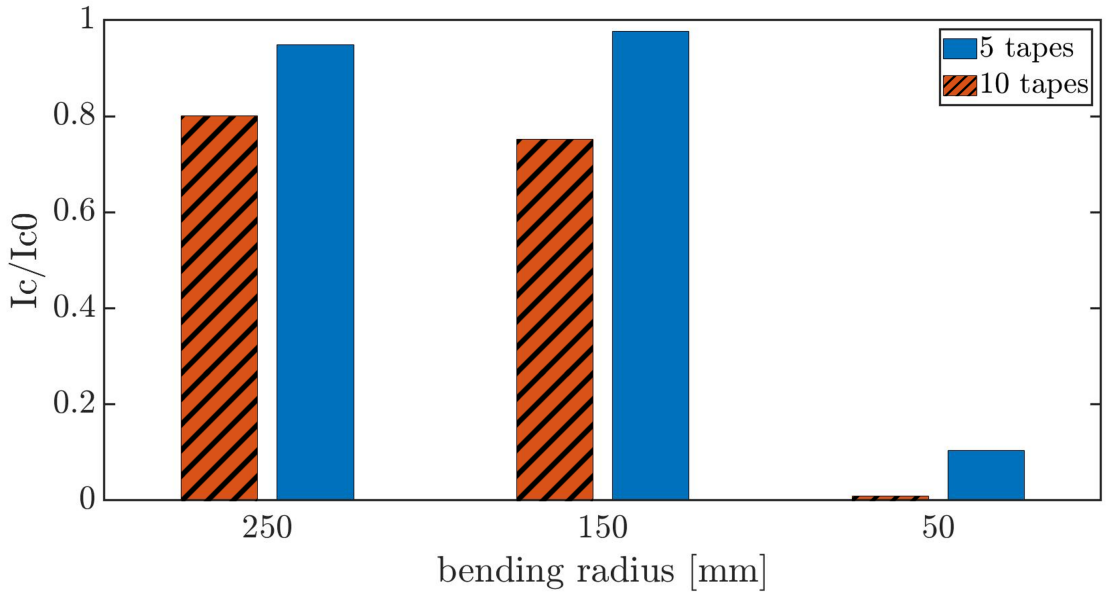

Figure (5.7) *Comparison between the 5-tape stack and 10-tape stack on the critical current degradation for the three different radii.*

5.5 Improvements

Even though the experiments were successful, there were still multiple parts that could be tackled differently.

First of all, in the soldering process, it is important to clean the tapes and the solder before putting them in the soldering tool. Cleaning with isopropanol ensures that there is no grease on the surface which improves the connection between the tapes and the solder. Additionally, applying flux to the tapes results in a better soldering process by removing metal-oxide layers on the surface. These measures were taken during the formation of the 10-stack cable resulting in a solid cable.

Secondly, the set-up could be improved by adding extra voltage taps and by adding a concave wooden plate. Extra voltage taps, for example on a smaller part of the arched part of the cable, could improve the understanding of the critical current distribution in the cable. Voltage taps can be placed such that the damages are outside the taps to measure the highest critical current. Furthermore, a concave wood piece with a radius that is equal to the outer radius of the cable could be used instead of the clamps. This could add to the set-up as it could ensure that the cable is bent with equal pressure along the cable. Also, it can keep the cable in place with less pressure than the clamps that were used in this experiment.

6 Conclusions and Further Research

In conclusion, this research showed that a stack cable containing more tapes experiences more critical current degradation than a stack with fewer tapes. The 5-tape stack showed limited degradation (2-5%) for the bending radii of 250 mm and 150 mm. The cable broke after bending it at a radius of 50 mm with only 10% critical current remaining. The 10-tape stack had severe critical current degradation (20-25%) for the radii of 250 mm and 150 mm and also broke when bent at the radius of 50 mm with only 1% critical current remaining. Bending at 50 mm also caused visual damage to both cables. Detachment at the soldered interface and buckling of the inner tapes was observed. This damage caused that the stack was not bent as a whole, without sliding between the tapes, as was assumed in the calculations

With these results, it is not possible to say whether the used estimations are accurate for soldered stack cables. The results were quite as expected but more bending radii are required to understand the dependence of the critical current degradation on the bending radii. Additionally, experiments with stacks that contain more tapes should be performed. This will give a better comparison to the stacks used in the target and capture magnet of the muon collider and better understand the dependence of the amount of tapes on the critical bending radius.

This experiment also showed that the used soldering process was successful and resulted in a solid stack cable without critical current degradation. The solder was also distributed equally with a total solder thickness of 100 to 200 µm along the cables. Only in the middle part of the 10-tape stack there was less solder (total of 30 µm thickness). Whether this type of solder is the best to handle large mechanical stresses is a topic of further research. In the experiment, the cable broke at the solder in both cases, so it seems like InSn solder is not strong enough. Not soldering the tapes to each other and letting them slide is also an option to consider.

7 Acknowledgements

I am extremely thankful for all the people that helped me during this thesis. First of all, I would like to express my appreciation to the chair of my committee Anna Kario for challenging me and for her always quick and valuable feedback. Additionally, I am grateful to my daily supervisor Simon Otten for providing his knowledge and expertise. I also could not have undertaken this journey without Jorick Leferink, who helped me with performing the experiments and was always optimistic even when things went wrong. Thanks should also go to my external supervisor Arie van Houselt for being enthusiastic to learn about new topics.

I am also thankful for the whole EMS research group for welcoming me with open arms and sharing their knowledge with me. In particular, I would like to thank Sander Wessel for arranging all the equipment and an excellent space to work.

I am also grateful to my classmates, and especially my Preparation Bachelor Assignment group, for their tips and moral support. Additionally, I would like to thank Daniel Chehata Gomez for helping me start up my thesis. Thanks should also go to the TCO lab employees and other university staff for providing me with the needed materials and equipment.

Lastly, I would be remiss in not mentioning my family, partner and friends. Their belief in me has kept me motivated during this process. They were always there to give tips and moral support.

References

[1] Wikimedia Commons. Standard model of elementary particles, 2019.

[2] CERN. Muon collider. Retrieved from www.home.cern/science/accelerators/muon-collider.

[3] C. Aime, A. Apyan, M. Mahmoud, N. Bartosik, A. Bertolin, M. Bonesini, S. Bottaro, D. Buttazzo, R. Capdevilla, M. Casarsa, et al. Muon collider physics summary. *arXiv preprint arXiv:2203.07256*, 2022. DOI: www.doi.org/10.48550/arXiv.2203.07256.

[4] International Muon Collider Collaboration. Overview. Retrieved from www.muoncollider.web.cern.ch/node/25.

[5] L. Bottura, D. Aguglia, B. Auchmann, T. Arndt, J. Beard, A. Bersani, F. Boattini, M. Breschi, B. Caiffi, X. Chaud, et al. A work proposal for a collaborative study of magnet technology for a future muon collider. *arXiv preprint arXiv:2203.13998*, 2022. DOI: www.doi.org/10.48550/arXiv.2203.13998.

[6] S. Kahn, M. Alsharo'a, R. Johnson, M. Kuchnir, R. Gupta, R. Palmer, E. Willen, and D. Summers. A high field hts solenoid for muon cooling. In *2007 IEEE Particle Accelerator Conference (PAC)*, pages 446–448. IEEE, 2007. DOI: www.doi.org/10.1109/PAC.2007.4440240.

[7] D. Stratakis, N. Mokhov, M. Palmer, N. Pastrone, T. Raubenheimer, C. Rogers, D. Schulte, V. Shiltsev, J. Tang, A. Yamamoto, et al. A muon collider facility for physics discovery. *arXiv preprint arXiv:2203.08033*, 2022. DOI: www.doi.org/10.48550/arXiv.2203.08033.

[8] L. Bottura et al. Muon collider magnets, March 2023. On behalf of the Muons Magnets Working Group.

[9] L. Bottura, C. Accettura, A. Kolehmainen, J. Lorenzo Gomez, A. Portone, and P. Testoni. Design and analysis of a hts internally cooled cable for the muon collider target magnet, 2023.

[10] M. Wilson. *Superconducting magnets*. 1983. ISBN: 978-0198548102.

[11] D. Uglietti. A review of commercial high temperature superconducting materials for large magnets: from wires and tapes to cables and conductors. *Superconductor Science and Technology*, 32(5):053001, 2019. DOI: www.doi.org/10.1088/1361-6668/ab06a2.

[12] A. Bussmann-Holder and H. Keller. High-temperature superconductors: underlying physics and applications. *Zeitschrift für Naturforschung B*, 75(1-2):3–14, 2020. DOI: www.doi.org/10.1515/znb-2019-0103.

[13] A. Kario. Superconducting matter(s) smashers, 2023.

[14] C. Barth, G. Mondonico, and C. Senatore. Electro-mechanical properties of rebco coated conductors from various industrial manufacturers at 77 k, self-field and 4.2 k, 19 t. *Superconductor Science and Technology*, 28(4):045011, 2015. DOI: www.doi.org/10.1088/0953-2048/28/4/045011.

[15] Z. Zhang, K. Wang, X. Wang, S. Chen, H. Suo, L. Ma, J. Liu, L. Wang, and Q. Wang. Effect of the cu stabilisation layer on the turn-to-turn contact resistance of a non-insulated rebco winding. *Physica C: Superconductivity and its Applications*, 590:1353949, 2021. DOI: www.doi.org/10.1016/j.physc.2021.1353949.

[16] K. Tsuchiya, A. Kikuchi, A. Terashima, K. Norimoto, M. Uchida, M. Tawada, M. Masuzawa, N. Ohuchi, X. Wang, T. Takao, et al. Critical current measurement of commercial rebco conductors at 4.2 k. *Cryogenics*, 85:1–7, 2017. DOI: www.doi.org/10.1016/j.cryogenics.2017.05.002.

[17] L. Monzon and J. Coey. Magnetic fields in electrochemistry: The lorentz force. a mini-review. *Electrochemistry Communications*, 42:38–41, 2014. DOI: www.doi.org/10.1016/j.elecom.2014.02.006.

[18] V. Fry, J. Estrada, P. Michael, E. Salazar, R. Vieira, and Z. Hartwig. Simultaneous transverse loading and axial strain for rebco cable tests in the sultan facility. *Superconductor Science and Technology*, 35(7):075007, 2022. DOI: www.doi.org/10.1088/1361-6668/ac6bcc.

[19] D. van der Laan, J. Ekin, J. Douglas, C. Clickner, T. Stauffer, and L. Goodrich. Effect of strain, magnetic field and field angle on the critical current density of y ba2cu3o7- δ coated conductors. *Superconductor Science and Technology*, 23(7):072001, 2010. DOI: www.doi.org/10.1088/0953-2048/23/7/072001.

[20] J. Weiss, T. Mulder, H. ten Kate, and D. van der Laan. Introduction of corc® wires: highly flexible, round high-temperature superconducting wires for magnet and power transmission applications. *Superconductor science and technology*, 30(1):014002, 2016. DOI: www.doi.org/10.1088/0953-2048/30/1/014002.

[21] M. Takayasu, L. Chiesa, L. Bromberg, and J. Minervini. Hts twisted stacked-tape cable conductor. *Superconductor Science and Technology*, 25(1):014011, 2011. DOI: www.doi.org/10.1088/0953-2048/25/1/014011.

[22] M. Takayasu, F. Mangiarotti, L. Chiesa, L. Bromberg, and J. Minervini. Conductor characterization of ybco twisted stacked-tape cables. *IEEE transactions on applied superconductivity*, 23(3):4800104–4800104, 2012. DOI: www.doi.org/10.1109/TASC.2012.2234182.

[23] Y. Pan and P. Gao. Analysis of mechanical behavior and electromechanical properties of rebco-coated conductor tapes under combined bending-tension loads using numerical methods. *Superconductor Science and Technology*, 36(4):045006, 2023. DOI: www.doi.org/10.1088/1361-6668/acbac7.

[24] W. Pi, Z. Sun, Z. Zhang, Y. Yang, R. Wang, S. Ma, and Y. Wang. Strain distribution and critical current characteristics of an individual rebco tape and quasi-isotropic superconducting strand under bending loads by the layerwise theory. *IEEE Transactions on Applied Superconductivity*, 32(6):1–7, 2022. DOI: www.doi.org/10.1109/TASC.2022.3150648.

[25] S. Otten, A. Kario, A. Kling, and W. Goldacker. Bending properties of different rebco coated conductor tapes and roebel cables at t= 77 k. *Superconductor Science and Technology*, 29(12):125003, 2016. DOI: www.doi.org/10.1088/0953-2048/29/12/125003.

[26] Y. Shi, S. Dai, T. Ma, and W. Liu. Effect of bending strain on the current-carrying performance of copper-laminated rebco tape. *Journal of Superconductivity and Novel Magnetism*, pages 1–9, 2022. DOI: www.doi.org/10.1007/s10948-021-06103-6.

[27] C. Zhou, K. Yagotintsev, P. Gao, T. Haugan, D. van Der Laan, and A. Nijhuis. Critical current of various rebco tapes under uniaxial strain. *IEEE transactions on applied superconductivity*, 26(4):1–4, 2016. DOI: www.doi.org/10.1109/TASC.2016.2535202.

[28] R. He, Y. Tan, Z. Huang, Y. Xie, G. Wang, Y. Wang, Q. Wu, and J. Wei. Bending and uniaxial tensile strain effects on the critical current of rebco coated conductor tapes. *Cryogenics*, 116:103285, 2021. DOI: www.doi.org/10.1016/j.cryogenics.2021.103285.

[29] G. De Marzi, N. Allen, L. Chiesa, G. Celentano, M. Takayasu, G. Tomassetti, A. Augieri, and A. Della Corte. Bending tests of hts cable-in-conduit conductors for high-field magnet applications. *IEEE Transactions on Applied Superconductivity*, 26(4):1–7, 2016. DOI: www.doi.org/10.1109/TASC.2016.2528501.

[30] Y. Shi, F. Liu, H. Liu, Y. Tan, X. Zhang, H. Jin, M. Yu, L. Lei, and L. Guo. Quasi-round hts conductor using rebco tapes for fusion magnet application. *IEEE Transactions on Applied Superconductivity*, 30(1):1–4, 2019. DOI: www.doi.org/10.1109/TASC.2019.2931998.

[31] Y. Wang, S. Baasansuren, C. Xue, and T. Hasegawa. Development of a quasi-isotropic strand stacked

by 2g wires. *IEEE Transactions on Applied Superconductivity*, 26(4):1–6, 2016. DOI: www.doi.org/10.1109/TASC.2016.2527042.

[32] A. Vaskuri, B. Curé, A. Dudarev, and M. Mentink. Aluminium-stabilized high-temperature superconducting cable for particle detector magnets. *IEEE Transactions on Applied Superconductivity*, 33(5):1–6, 2023. DOI: www.doi.org/10.1109/TASC.2023.3262770.

[33] C. Senatore, M. Bonura, T. Bagni, and D. Zurmuehle. Introduction to the activities of the wp2.3 at unige: Focus on rebco coated conductors.

[34] SuperOx GdBCO 2G HTS, Feb 2021. Retrieved from Robinson HTS Wire Critical Current Database: www.htsdb.wimbush.eu/dataset/3759315.